Langmuir

Article

pubs.acs.org/Langmuir

Modification of Tethered Bilayers by Phospholipid Exchange with Vesicles

Rima Budvytyte,[†] Mindaugas Mickevicius,[†] David J. Vanderah,[‡] Frank Heinrich,[§,∥] and Gintaras Valincius*[,†]

[†]Institute of Biochemistry, Vilnius University, Vilnius LT-08662, Lithuania

[‡]Institute for Bioscience and Biotechnology Research, National Institute of Standards and Technology (NIST), Rockville, Maryland 20850, United States

[§]Department of Physics, Carnegie Mellon University, Pittsburgh, Pennsylvania 15213, United States

[∥]National Institute of Standards and Technology (NIST) Center for Neutron Research, Gaithersburg, Maryland 20899, United States

Supporting Information

ABSTRACT: Phosphatidylcholine and cholesterol exchange between vesicles and planar tethered bilayer lipid membranes (tBLMs) was demonstrated from electrochemical impedance spectroscopy (EIS), fluorescence microscopy (FM), and neutron reflectometry (NR) data. Cholesterol is incorporated into the tBLMs, as determined by the functional reconstitution of the pore forming toxin α-hemolysin (EIS data), attaining cholesterol concentrations nearly equal to that in the donor vesicles. Using fluorescently labeled lipids and cholesterol, FM indicates that the vesicle−tBLM exchange is homogeneous for the lipids but not for cholesterol. NR data with perdeuterated lipids indicates lipid exchange asymmetry with two lipids exchanged in the outer leaflet for every lipid in the inner leaflet. NR and EIS data further show different exchange rates for cholesterol ($t_{1/2}$ < 60 min) and phosphatidylcholine ($t_{1/2}$ > 4 h). This work lays the foundation for the preparation of robust, lower defect, more biologically relevant tBLMs by essentially combining the two methods of tBLM formation−rapid solvent exchange and vesicle fusion.

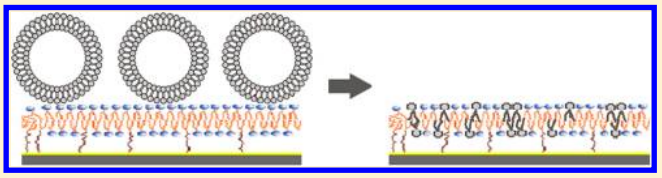

INTRODUCTION

Solid-supported membrane models are extensively used to study the physical and chemical processes occurring in biological membranes, such as the structure−function relationship of membrane proteins, molecular recognition, membrane permeation, signaling, adhesion, and fusion.[1−4] Current models include freely-suspended phospholipid bilayer membranes (FSPBMs),[5,6] polymer-cushioned bilayer lipid membranes,[7] hybrid bilayer membranes (HBMs),[8] and tethered bilayer lipid membranes (tBLMs).[9−12] FSPBMs and HBMs are formed by either a sequential transfer of phospholipid layers from an air/water interface[5,8] or the fusion of vesicles to an appropriate solid substrate.

The tBLMs are anchored to the solid surface by synthetic lipidic anchor molecules.[11−13] Hydrophobic segments of the anchor intercalate into the core of the phospholipid bilayer, while a hydrophilic segment holds the bilayer at some distance (typically 1−2 nm) from the surface, providing a water-filled reservoir to accommodate extra-membranous protein sequences. Each type of solid-supported membrane model has its advantages and drawbacks. tBLMs, in comparison to FSPBMs, exhibit increased temporal stability[14] and low defectiveness[15] and are highly electrically resistive, important in practical applications, such as biosensors.[16]

The tBLMs can be completed by either rapid solvent exchange (RSE) or vesicle fusion. In the RSE method, the substrate is first coated with a self-assembled monolayer (SAM). The SAM-coated substrate is then immersed in a solution of lipids, in a water miscible solvent, such as ethanol or methanol, followed by rapid displacement with buffer. In the vesicle fusion method, the SAM-coated surface is immersed in a buffer solution containing vesicles of a lipid or lipid mixture that may contain proteins or peptides. However, as we recently observed, complete, vesicle-fused, as determined by neutron reflectometry (NR), sparsely tethered tBLMs still exhibit a relatively high number of defects[17] and are unsuitable for applications requiring low residual conductivity membranes, such as the detection of toxins and bacteria.

To overcome these deficiencies, we were prompted to investigate the formation of tBLMs by a combination of RSE and vesicle fusion, i.e., to investigate material exchange between RSE-completed tBLMs and vesicles. In biology, material exchange between plasma membranes and various organelles is a common process.[18−20] Membrane fusion and material exchange is central to cellular secretion and endocytosis, infection of eukaryotic host cells by enveloped viruses, cell−cell fusion, etc.[21−24] The movement of cholesterol from donor to acceptor vesicles has been widely studied.[25,26] To the best of

Received: November 19, 2012
Revised: February 22, 2013
Published: February 27, 2013

our knowledge, the investigation of material exchange between vesicles and planar tBLMs has not been previously investigated. The main objective of the current work was to apply RSE to form a core surface tethered phospholipid bilayer and then follow its lipid material composition modification by exchange with the vesicles. We aimed also at establishing the extent of asymmetry that may be accomplished in such an exchange process.

MATERIALS AND METHODS

Materials. Mixed SAMs were prepared using either the synthetic lipidic anchor compound FC16 [29-hexadecyloxy-3,6,9,12,15,18,21,24,27,31-decaoxaheptatetracontan-1-thiol, C_{16}, palmitoyl][27] or HC18 [*Z*-20-(*Z*-octadec-9-enyloxy)-3,6,9,12,15,18,22-heptaoxatetracont-31-ene-1-thiol, C_{18}, oleoyl][17] with β-mercaptoethanol (βME). βME was purchased from Sigma-Aldrich (St. Louis, MO). The all hydrogen phospholipid 1,2-dioleoyl-*sn*-glycero-3-phosphocholine (DOPC or h-DOPC), 1,2-dipalmitoyl-*sn*-glycero-3-phosphoethanolamine-*N*-(lissamine rhodamine B sulfonyl) (ammonium salt) (LR-DOPE), 5-cholesten-3β-ol 6-[(7-nitro-2-1,3-benzoxadiazol-4-yl)-amino]caproate (chol-NDB), and the deuterated lipid dimyristoyl-*sn*-glycero-3-phosphocholine-d_{54} (DMPC-d_{54}) were used as purchased from Avanti Polar Lipids (Alabaster, AL). Ultrapure H_2O was obtained from a Millipore (Billerica, MA) UHQ reagent-grade water purification system.

tBLM Preparation. Silicon wafers, 76.2 mm in diameter (Silicon Quest International, Inc., Santa Clara, CA), were cleaned first with Hellmanex solution (Hellma GmbH, Müllheim, Germany), and later immersed for 15 min in Nochromix solution (Godax Laboratories, Inc., Cabin John, MD). After each step, the wafers were extensively rinsed with Millipore water. Clean wafers were coated with thin films of Cr (1 nm) and Au (45 nm) by magnetron sputtering (ATC Orion, AJA International, Inc., North Scituate, MA), then immediately after coating incubated for 12−18 h in a $c_{total} = 0.2 \times 10^{-3}$ mol/L ethanolic solution of tether and βME in a molar ratio of 30:70 using either FC16 or HC18. All tBLMs were initially prepared by the RSE technique.[12] Briefly, the SAM-coated Si/Au wafer was exposed to 0.01 mol/L solutions of either pure DOPC in ethanol or a mixture of DOPC and cholesterol in methanol. Rapid replacement of this solution followed using aqueous buffer (0.1 mol/L NaCl and 0.01 mol/L NaH_2PO_4 at pH 7.4).

Vesicle Preparation and Lipid Exchange with tBLMs. Vesicles were prepared using 0.01 mol/L solutions of 100% DOPC or mixtures of cholesterol and DOPC at a molar ratio of 30:70, in chloroform. The 30:70 ratio approximately mimics the neuronal membrane composition.[28] A lipid film was prepared by evaporating 1 mL of the chloroform solution in a gentle stream of nitrogen followed by vacuum drying for 1 h. The lipid film was redissolved in 1 mL of pentane and dried overnight. The film was hydrated by adding 2.5 mL of working buffer, 0.1 mol/L NaCl, and 0.5×10^{-3} mol/L NaH_2PO_4 (pH 7.4), sonicated for 60 min, and incubated with occasional vortexing, as needed, until the lipid film was no longer visible. The lipid preparation was then extruded 21 times through a 100 nm polycarbonate membrane (Avanti Polar Lipids, Alabaster, AL). The vesicle size distribution was single-peaked at ≈50 nm, as determined by dynamic light scattering. For lipid exchange, tBLMs were exposed for 1 h to an excess of vesicles using a 5 mg/mL vesicle solution.

Electrochemical Impedance Spectroscopy (EIS). EIS was performed with a Solartron 1287A and a 1260 frequency analyzer (Farnborough, U.K.), or a Parstat 2273 workstation (Princeton Applied Research, TN). The Au-coated silicon wafer (20 × 40 mm) serves as the working electrode in the electrochemical cell, which contains six distinct electrochemical cell volumes $V = \sim 300$ μL, with surface areas $A_{el} = 0.32$ cm^2 on the gold film defined by Viton O-rings. The reference electrode was a saturated silver−silver chloride [Ag/AgCl/$NaCl_{aq,sat}$] microelectrode (Microelectrodes, Bedford, NH, model M-401F), and the auxiliary electrode was a 0.25 mm diameter platinum wire (99.99% purity, Aldrich) coiled around the barrel of the reference electrode. The distance between the tip of the reference and working gold electrode surface was set to 2−3 mm. All measurements were carried out at 0 V bias versus the reference electrode at 21 ± 1 °C in aerated solutions. EIS spectra were normalized to the sample surface area and fitted to equivalent circuit models[9] using ZView (Scribner Associates, Southern Pines, NC).

Fluorescence Microscopy (FM). Vesicles of 30:70 molar ratio of cholesterol/DOPC were spiked with 0.06% LR-DOPE and/or 0.03% chol-NDB. FM images were obtained on an Axiotechvario (Carl Zeiss, Jena, Germany) epifluorescence microscope outfitted with an EM-CCD model C9100 video camera (Hamamatsu Photonics, Herrsching, Germany) and Zeiss Water Achroplan (20×/0.5 NA) objective lens. Zeiss filter sets 14 and 10 were used to image the lateral distribution of LR-DOPE and chol-NDB, respectively. Lipid exchange experiments were performed in a Nunc Lab-Tek chambered cover glass (Thermo Fisher Scientific, Rochester, NY) sample cell, using 5 × 5 mm samples with RSE tBLMs resting at the bottom without fixation. All images were taken after extensive washing with vesicle-free buffer.

NR. Silicon wafers, 76.2 mm in diameter and 6 mm thick (El-Cat, Inc., Waldwick, NJ), were coated with thin films of chromium (≈4 nm) and gold (≈15 nm) using a Denton Discovery 550 sputtering instrument (Denton Vacuum LLC, Moorestown, NJ) then immediately incubated in a HC18/βME solution in absolute ethanol for 24 h. The tBLMs were completed using the RSE procedure described above. NR measurements were carried out at the ISIS Pulsed Neutron and Muon Source, Appleton Rutherford Laboratory (Oxfordshire, U.K.). The reflectometer Inter was used with a horizontal sample mounting configuration. Two data sets recorded at angles of incidence 0.70° and 2.4° were recorded to obtain reflectivity curves spanning the momentum transfer vector, Q_z, range from 0.01 to 0.30 Å^{-1}. Each sample condition was characterized using at least two isotopically different bulk solvents (H_2O- and D_2O-based buffer), exchanging the solvent *in situ* at the instrument without disassembly of the sample cell.

Data evaluation was carried out by fitting models of the surface structure to the experimental results. We use a composition-space model that parametrizes the interfacial structure in terms of molecular composition and connectivity and yields distributions of submolecular components across the interfacial region.[29] Reflectivity curves were fitted using the ga_refl software.[30] Confidence limits of the model parameter values were evaluated by Monte Carlo simulation[27] and are reported as 68% confidence intervals.

RESULTS

Cholesterol Transfer from Vesicles to tBLMs Observed by EIS. Figure 1A shows the complex capacitance plots of representative electrochemical impedance (EI) spectra of FC16 tBLMs that were completed with DOPC and increasing amounts of cholesterol using the RSE procedure. An increased cholesterol content leads to a decrease in the semicircular part of the complex capacitance spectra, reflecting a significant decrease in tBLM capacitance of the membrane. Fitting the semicircular parts of the spectra to a series resistance, *R*, and constant phase element, *Q*, equivalent model (*RQ*), written here according to the Boukamp notation,[31] yields the *Q* values of the tBLMs. The constant phase element is an electric element, in which impedance is defined as $Z = (Q)^{-1}(j\omega)^{-\alpha}$, where *Q* is the constant phase element coefficient, ω is the cyclic frequency, and *j* is the imaginary unit. When the exponent of a constant phase element α is close to 1, as is the case in these systems (see Table 1), *Q* may be regarded as the capacitance. In our case, this is a capacitance C_{mH}, which integrates the dielectric properties of both the phospholipid membrane and the Helmholtz layer[28] (see the Supporting Information for the definition of C_{mH}). A plot of C_{mH} as a function of the cholesterol mole fraction (Figure 1B) shows that, from 0 to 40% cholesterol content, the capacitance decreases almost linearly from ≈0.8 to ≈0.5 μF/cm^2. From 50

dx.doi.org/10.1021/la304613a | *Langmuir* 2013, 29, 4320−4327

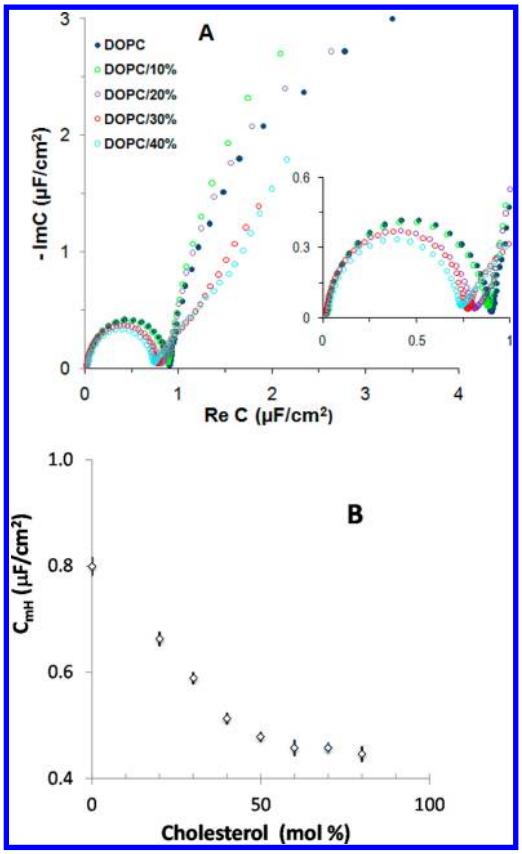

Figure 1. (A) Complex capacitance plots of the EI spectra of 100% DOPC- and cholesterol/DOPC-completed 30% FC16 tBLMs as a function of an increasing cholesterol concentration: 0% (blue), 10% (green), 20% (purple), 30% (red), and 40% (light blue). (Inset) Expanded view of the high-frequency range of the plot. The data were normalized with respect to the geometric surface area (*a*). (B) Capacitance of the 30% FC16 tBLMs as a function of the cholesterol concentration in ethanol solution used for RSE. The data were normalized with respect to the geometric surface area. The surface roughness factor is 1.39.

to 80% cholesterol content, it decreases more slowly to ≈0.45 μF/cm^2.

The complex capacitance EI spectra of 100% DOPC and 30% cholesterol/DOPC tBLMs completed by RSE on the HC18 anchor (Figure 2A) exhibit the same features observed for tBLMs on FC16 anchor (Figure 1A). In particular, the introduction of 30% cholesterol into the tBLM decreases the diameter of the semicircular part of the EI spectra by about 30%, which is equivalent to a decrease of C_{mH} by the same amount as seen in Figure 2A. This indicates that the cholesterol effect on capacitance is independent of the anchor and is primarily the related to the introduction of cholesterol into the bilayer.

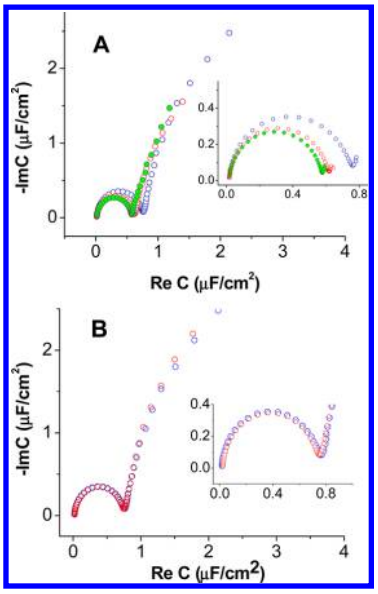

Figure 2. Complex capacitance plots of the EI spectra of tBLMs prepared on 50% HC18 SAMs and completed by RSE with (A) 30% cholesterol/DOPC (green), DOPC (blue), and DOPC and then exposed to 30% cholesterol/DOPC vesicles (red) and (B) DOPC (blue) and DOPC and then exposed to 100% DOPC vesicles (red). All spectral changes occurred within 40−60 min. Extension of the incubation with the vesicle solution to 90 min did not cause further significant changes in EI spectra (data not shown). The data were normalized with respect to the geometric surface area. The surface roughness factor is 1.39.

Exposure of 100% DOPC HC18 tBLMs to a solution of 30% cholesterol/DOPC vesicles results in an EI spectrum change nearly identical to that of the tBLM completed with the 30% cholesterol/DOPC lipid mixture by RSE (red and green curves in Figure 2A). Exposure to cholesterol-free DOPC vesicles, however, shows only marginal changes (Figure 2B). Fitting the semicircular parts of the Figure 2A spectra, as described for the spectra in Figure 1A, shows a significant capacitance decrease ($\Delta C_{mH} \approx -0.15$ μF/cm^2; Table 1) from the interaction of the tBLMs with the cholesterol-containing vesicles. Therefore, the EI spectral variations seen in Figure 2A may be directly attributed to an uptake of cholesterol transferred from the vesicles to the planar tBLM.

In addition, the similar capacitance values of the planar tBLMs, after exchange with the cholesterol/DOPC vesicles, to that of the RSE cholesterol/DOPC-completed tBLMs (Table 1) indicate similar cholesterol compositions. Subtle changes in the variation of α are noted. The introduction of cholesterol into the tBLMs was accompanied by a shift of α values toward 1. In the control experiment (Figure 2B) only a marginal decrease in C_{mH} ($\Delta C_{mH} = -0.03$ μF/cm^2) is observed, with no shift in α.

Table 1. Electrochemical Parameters of tBLMs Calculated from the Complex Capacitance Plots in Figure 2[a]

EIS parameters	DOPC HC18 tBLM by RSE	cholesterol/DOPC tBLM by RSE	after 1 h of exposure to DOPC vesicles	after 1 h of exposure to 30% cholesterol/DOPC vesicles
C_{mH} (μF/cm^2)	0.84 ± 0.02	0.61 ± 0.02	0.81 ± 0.03	0.69 ± 0.01
α_{mH}	0.976 ± 0.002	0.990 ± 0.001	0.975 ± 0.002	0.989 ± 0.002

[a]Capacitance was normalized to a geometric surface area. The roughness factor of the electrodes was ∼1.4. Average parameters and standard errors were obtained from three measurements.

dx.doi.org/10.1021/la304613a | *Langmuir* 2013, 29, 4320−4327

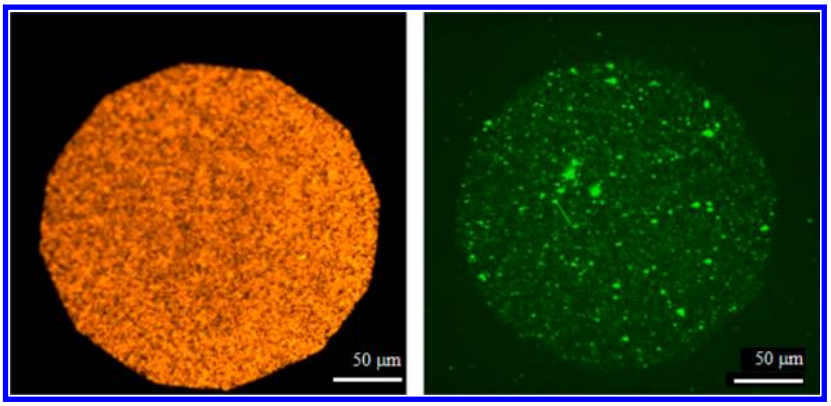

Figure 3. Fluorescence micrographs of DOPC-completed 30% HC18 tBLMs after exchange with fluorescently labeled 30% cholesterol/DOPC vesicles containing (left panel) 0.06% LR-DOPE and (right panel) 0.03% chol-NDB.

Cholesterol Transfer from Vesicles to tBLMs Observed by FM. The transfer of cholesterol and phospholipids from vesicles to tBLMs is also seen in the fluorescence micrograph images (Figure 3) of DOPC-completed HC18 tBLMs after exposure to cholesterol/DOPC vesicles containing LR-DOPE (left panel) and chol-NBD (right panel), at 0.06 and 0.03%, respectively. Transfer of LR-DOPE and chol-NBD is clearly evident with a more even distribution for LR-DOPE, as might be expected. Exposure of an as-prepared tBLM to vesicles containing both LR-DOPE and chol-NBD gave similar results to those in Figure 3 with uneven ("patchy") images for both (see Figure S2 in the Supporting Information). The images, obtained without moving the sample, indicate essentially no common patches, suggesting little or no co-precipitation of cholesterol and DOPC onto the tBLM surface.

Cholesterol Transfer from Vesicles to tBLMs Facilitates the Reconstitution of α-Hemolysin (αHL). Figure 4 shows the EI spectral changes of DOPC-completed HC18 tBLMs to a 140 nM solution of αHL after 60 min with and without prior exposure to cholesterol/DOPC vesicles. The EI spectral changes are dramatically different. Prior exposure to the cholesterol/DOPC vesicles (open circle data) leads to EI changes consistent with the incorporation of αHL.[33] Estimates made from the analysis of EI spectra in Figure 4 according to recent formalism[32] indicate the αHL channel density as high as ~10 μm^{-2} (see the Supporting Information). In stark contrast, exposure of the as-prepared, cholesterol-free DOPC tBLMs to αHL shows essentially no changes (filled circle data). These results not only confirm cholesterol transfer from vesicles to tBLMs but also show the more facile reconstitution of αHL with cholesterol in the bilayer environment.

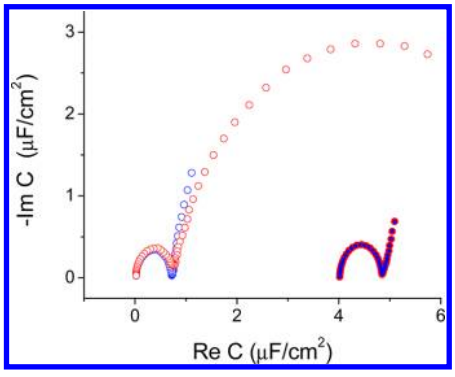

Figure 4. Complex capacitance plots of EI spectra of DOPC completed HC18 tBLMs prior (solid blue) and after (solid red) to exposure to 140 nM αHL and DOPC completed HC18 tBLMs exposed to cholesterol/DOPC vesicles for 60 min prior (open blue) and after (open red) exposure to 140 nM αHL. Solid circle data are offset by 4 mF/cm^2 along the Re C axis for clarity. The data were normalized with respect to the geometric surface area. The surface roughness factor is 1.39.

NR Reveals Material Distribution in the Inner and Outer Leaflets of the tBLMs. NR provides data on compositional and structural features in tBLMs. The continuous distribution profiles of materials and components in h-DOPC-completed HC18 tBLMs are shown in Figure 5A. The corresponding fitted parameters are summarized in Table 2 (see Supporting Information for NR curves and neutron scattering length density profiles and also a full set of fitted parameters used in the modeling). The completeness of the h-DOPC HC18 tBLM was 96 ± 2% (average value obtained from pristine and vesicle treated tBLM data). The bilayer thickness was 3.1 ± 0.2 nm (average value obtained from pristine and vesicle treated tBLM data), matching previously obtained thicknesses of 3.1 ± 0.1 nm.[17,34] However, this sample exhibited a larger ethylene oxide (EO)-tether thickness of d_{tether} = 1.4 ± 0.1 nm and a lower βME/tether molar ratio of 1.3 ± 0.8 than previously obtained for 30% HC18 tBLMs, with d_{tether} = 1.1 nm and 2.4, respectively.[17] The ratio of 1.3 constitutes a βME/tether surface ratio of ~57:43, which is different from the 70:30 ratio of the mixed SAM-forming solution. For this HC18 tBLM, the inner hydrophobic leaflet of the bilayer contains a 0.84 ± 0.10 mol fraction of dioleoyl chains that belong to the HC18 anchor compound (Table 2) and only a 0.16 ± 0.10 mol fraction of exchangeable dioleoyl chains (the mole fraction of the exchangeable alkyl chains of the outer hydrophobic leaflet is 1).

The exposure of the h-DOPC-completed tBLM to DMPC-d_{54} vesicles results in noticeable changes in the material distribution in the hydrophobic segments of the tBLM. Profiles of deuterated material are evident in Figure 5B. Integration of volume fraction curves in Figure 5 indicates that 90 min of interaction between the tBLM and the vesicles was sufficient to exchange ~22% of h-DOPC with DMPC-d_{54} (Table 2) in the outer leaflets of tBLMs and ~53% of h-DOPC with DMPC-d_{54} in the inner leaflets of tBLMs.

DISCUSSION

Cholesterol Transfer Decreases the Capacitance of DOPC tBLMs. The experimentally observed (panels A and B of

dx.doi.org/10.1021/la304613a | Langmuir 2013, 29, 4320−4327

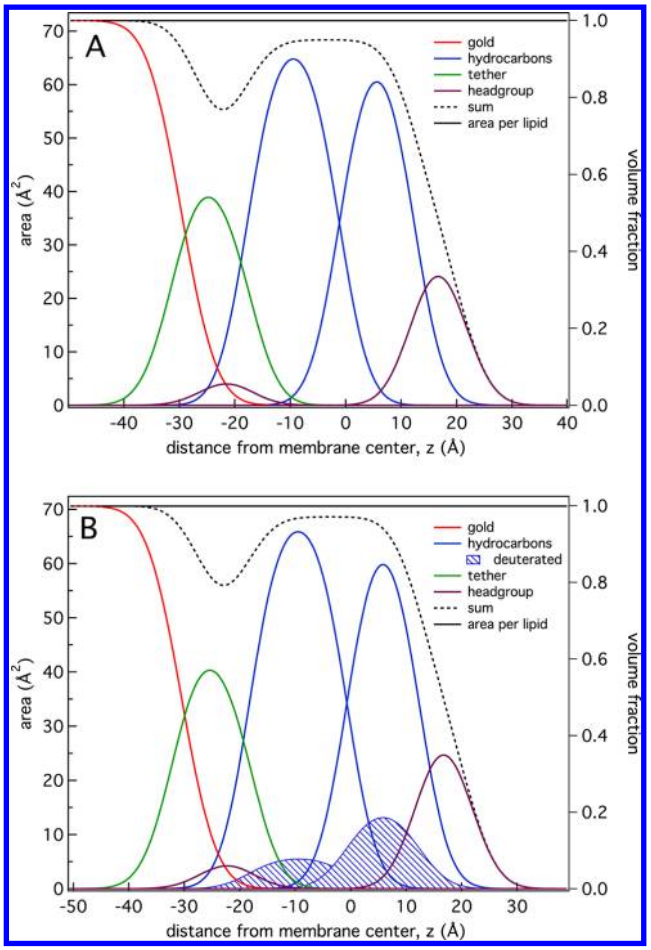

Figure 5. Best-fit volume occupancy profiles for the molecular components for a h-DOPC-completed tBLM: (A) as-prepared with RSE and (B) after addition of DMPC-d_{54} vesicles. The shaded areas represent the deuterated fraction of the hydrocarbon material.

Table 2. Parameters Obtained from the Fit of the NR Data to a Model[a]

physical property	values	
	pristine bilayer	after exposure to vesicle solution
thickness of the tether (Å)	$13.8^{+0.9}_{-0.8}$	$12.9^{+1.2}_{-1.4}$
molar fraction of tether in the inner lipid leaflet	$0.84^{+0.07}_{-0.10}$	
number of βME molecules per tether molecule	$1.3^{+0.5}_{-0.6}$	
thickness of the inner lipid leaflet (Å)	$16.4^{+0.8}_{-0.6}$	$17.6^{+1.1}_{-1.1}$
thickness of the outer lipid leaflet (Å)	13.4 (fixed)	$12.9^{+0.8}_{-0.9}$
molar fraction of deuterated lipid material (not tether) in the inner lipid leaflet		$0.54^{+0.21}_{-0.21}$
molar fraction of deuterated lipid material in the outer lipid leaflet		$0.22^{+0.03}_{-0.03}$
completeness of the bilayer	$0.95^{+0.02}_{-0.02}$	$0.97^{+0.02}_{-0.02}$
best-fit χ^2	3.27	

[a]Uncertainties represent 68% confidence limits.

Figure 1) capacitance decrease by cholesterol may be purely phenomenological. Density of pores in phospholipid bilayers are determined by the standard free energy of pore formation, which depends upon the line tension along the rim of the pore. Cholesterol increases the line tension.[35] Thus, the presence of cholesterol in the methanolic phospholipid solution may affect the RSE process itself; i.e., it may result in less defective tBLMs. Similarly, transfer of cholesterol from vesicles may reduce the pore density. While we cannot exclude such phenomena taking place during the material exchange with vesicles, the estimates based on theoretical analysis (see eq 29 in ref 32 and also see the Supporting Information) show that noticeable capacitance decreases, such as observed in the current work (Table 1), will be observed only if the defect (pore) density in the pristine tBLM is very high, with membrane-free patches on the surface comprising at least 15−20% of the total surface area. An estimate based on data in Figure 2 (blue symbols, pure DOPC tBLM EI spectrum) indicates that defect density is <1 μm^{-2} and the membrane-free fraction of the surface is $\ll$1%. Therefore, change in tBLM defectiveness is excluded as a primary reason for the observed capacitance decrease.

The effect of cholesterol on the capacitance of bilayer membrane systems is controversial. For black lipid membranes (BLMs) some reports indicate an increase in capacitance[36] with the addition of cholesterol and others indicate the opposite.[37] In this work, the increasing cholesterol resulted in a decreasing capacitance, C_{mH}, of the RSE-completed tBLMs (panels A and B of Figure 1). Although a compound parameter, the major contributor to C_{mH} is the bilayer, C_m (eq 1), where ε and ε_0 are the relative dielectric constants of the bilayer and the vacuum constant, respectively, and h is the thickness of the dielectric sheet. Apparent from eq 1 is that capacitance will decrease if h increases or ε decreases.

$$C_m = \frac{\varepsilon\varepsilon_0}{h} \quad (1)$$

Recent X-ray diffraction (XRD) measurements on stacked lipid bilayers[38,39] indicate a thickness increase of DOPC bilayers by a factor of 1.10, in the presence of 40% cholesterol, with an estimated thickness increase of the hydrophobic core, contributing the most to C_m, by a factor of 1.12−1.14. Such a contribution, however, is too small to account for the observed capacitance decrease, which, for 30% cholesterol tBLMs accomplished by RSE and vesicle transfer, comprises a factor of 1.38 and 1.22, respectively, as estimated from the data in Table 1.

The dielectric constant ε is another parameter that may affect measured C_{mH} capacitance and its major contributor C_m. Because of the dipole moment of cholesterol[40] (μ = 2 D), insertion into tBLMs could increase ε. However, contributions to ε are considerable only if the dipolar molecule reorientation motion is sufficiently facile to keep up with the polarizing alternating electric field, which in our case was >1000 Hz. The experimental estimates of the intramembrane (flip-flop) mobility of cholesterol are controversial, with the relaxation times of the process spanning from <10 ms[41] and <1 s[42] to >3 h[43] and, although a large range, well above that needed at frequencies >1000 Hz. Thus, we believe cholesterol dipole contribution increasing ε should be minimal.

The XRD data also show that, at 40% cholesterol, the apparent area per DOPC molecule decreases from 73 ± 1 to 65 ± 1 Å^2 (a factor of ≈1.11)[38] or even to 54 ± 1 Å^2 (a factor of ≈1.37).[39] It is also known that cholesterol, in the biologically relevant liquid crystalline state, exhibits an ordering effect of phospholipids and decreases the membrane permeability of polar molecules.[44,45] Such effects would diminish the concentration of voids and exclude residual polar components, such as H_2O, from the hydrophobic core of the membrane, thus

dx.doi.org/10.1021/la304613a | Langmuir 2013, 29, 4320−4327

decreasing ε. The relative dielectric constant of a DOPC bilayer is $\varepsilon \approx 2.8$.[34] Assuming a minimum value of $\varepsilon \approx 2.0$ (a value for saturated hydrocarbons), the capacitance should decrease by a factor of 1.40 because of variations of the relative dielectric constant. Consequently, changes in two factors, the bilayer thickness and the relative dielectric constant, could result in C_{mH} decreases by a factor of 1.60, which is more than enough to account for the observed variation of C_{mH} (Table 1). Notably, a sharp decrease of C_{mH} is observed in the cholesterol concentration interval from 0 to 40%. As demonstrated earlier,[39] at concentrations above 40%, cholesterol phase-separates from DOPC. As a result, one may expect that the physical properties of DOPC bilayers, including thickness and relative dielectric constant, will continuously and dramatically change up to 40% cholesterol, and then the variation patterns should slow, when the phase separation starts, as observed in the current work (Figure 1B).

The change in capacitance of the DOPC tBLMs, after exposure to the cholesterol/DOPC vesicles ($\Delta C_{mH} = -0.15$ $\mu F/cm^2$; Table 1) is significant compared to the marginal change obtained after exposure to cholesterol-free DOPC vesicles ($\Delta C_{mH} = -0.03$ $\mu F/cm^2$) and, thus, is attributed to vesicle−tBLM transfer of cholesterol. In addition, the parameter α_{mH}, reflecting the intrinsic heterogeneity of the tBLMs, is noticeably lower for the cholesterol-free tBLMs. The interaction of DOPC tBLMs with the cholesterol/DOPC vesicles results in α_{mH} parameter values approaching those for the RSE 30% cholesterol/DOPC-completed tBLMs (see Figure 1A) while remaining essentially unchanged after the interaction with cholesterol-free DOPC vesicles. This is in-line with an ordering effect of cholesterol discussed before (*vide supra*). Finally, we note, the cholesterol transfer occurs quite fast in experiments carried out at room temperature (20 °C). In ≈60 min of interaction between the 30% cholesterol/DOPC vesicles and the DOPC tBLMs, the capacitance decrease (−0.15 $\mu F/cm^2$) comprises almost 65% of that expected (−0.23 $\mu F/cm^2$), assuming that, upon reaching 30% in the tBLMs in the course of the cholesterol exchange, the capacitance of the latter would be the same as that of RSE 30% cholesterol/DOPC-completed tBLMs (0.61 $\mu F/cm^2$). From this, we conclude that the time of one-half of the possible cholesterol vesicle−tBLM transfer ($t_{1/2}$), from 0 to 30%, is <60 min, slower but comparable to that observed by small-angle neutron scattering for the cholesterol exchange between vesicles (88 ± 2 min).[43]

Cholesterol Phase-Separates When Transferred from Vesicles to tBLMs. The FM data provide direct confirmation of the transfer of lipids (DOPC) and cholesterol to the tBLMs (Figure 3). DOPC transfer occurs in the absence (Figure 3) and presence (see Figure S2 of the Supporting Information) of cholesterol in the donor vesicles. We did not detect any significant enhancement of the LR-DOPC signal when the cholesterol was present in the vesicles compared to when it was not, indicating that the phospholipid vesicle−tBLM transfer occurs independently from the cholesterol. The fluorescently labeled cholesterol images are more heterogeneous than the LR-DOPE images, with several micrometer-size fluorescent aggregates dominating the field, suggesting phase separation of cholesterol from the DOPC membrane. The FM experiment was carried out below a 40% fraction of cholesterol in DOPC, at which phase separation is observed in stacked bilayers.[39] Nevertheless, the heterogeneous distribution of cholesterol in tBLMs is obvious (Figure 3 and see Figure 2S in the Supporting Information). What is different in our work is the presence of oleoyl chains in the relatively immobile anchor molecules, which may alter the phase separation threshold in the cholesterol/DOPC system. How this affects cholesterol distribution requires further study, with our current data being the initial window into the effect that anchor molecules may have.

Activation of αHL Attests to the Cholesterol-Triggered Decrease of Polarity Inside the DOPC Membrane. While both the FM and EIS data attest to vesicle−tBLM material transfer, it is not clear whether the transferred cholesterol triggers functional changes in membranes. To demonstrate a biologically relevant change of the function of the phospholipid membrane in tBLM, we used the propensity of cholesterol-dependent cytolysins, such as αHL, to insert into cholesterol-rich bilayers, damaging their integrity and insulating capability by assembling into water-filled pores. Even though αHL has no strict requirement for cholesterol and reconstitutes into planar bilayers containing only phospholipids, such as diphytanoylphosphatidyl choline (DPhyPC),[46] its pore-forming ability is amplified by cholesterol.[47] In our experiments, we detected no αHL reconstitution into pure DOPC tBLMs. In contrast, the sequential addition of cholesterol/DOPC vesicles and, after the perfusion of the cell with vesicle-free buffer, the addition of αHL immediately triggered EI spectral changes, consistent with the formation of the water-filled pores of the toxin, as seen from spectra in Figure 4. Noteworthy, DPhyPC-completed tBLMs, which are easily damaged by αHL,[34] exhibit lower capacitance values compared to the αHL-resistant DOPC tBLMs. According to our earlier estimates,[32] the difference in capacitance values is due to a lower dielectric constant of the hydrophobic sheets in DPhyPC ($\varepsilon \approx 2.2$) and DOPC ($\varepsilon \approx 2.8$) tBLMs. We may to assume that the cholesterol, which is believed to lower the dielectric constant near the carbonyl groups inside the bilayer,[40] may, therefore, activate αHL reconstitution into the DOPC tBLMs. Activation of the αHL supports functional insertion of the cholesterol into the tBLMs via interaction with donor vesicles.

Lipid Material Transferred from Vesicles Is Distributed Asymmetrically in tBLMs. Along with other techniques used in the current study, lipid material transfer is also documented by the NR. The deuterated material profile displayed in Figure 5 clearly indicates an asymmetric distribution of vesicle material in the hydrophobic core of the tBLMs. As obvious from data in Table 2, the composition change occurs at different rates in the inner and outer leaflets of the bilayer. During 90 min of tBLM exposure to deuterated vesicle solution, the outer leaflet exchanged ≈22% of h-DOPC with DMPC-d_{54} (Table 2), while the inner leaflet exchanged ≈54%. However, the inner leaflet initially contains only 0.16 molar fraction of oleoyl chains of h-DOPC not conjugated to the tether molecules. Therefore, after the exchange with DMPC-d_{54} vesicles, the outer leaflet contains 0.22 DMPC-d_{54} phospholipid and the inner leaflet contains 0.09 DMPC-d_{54} phospholipid. From this, we deduce that the exchange of the lipid material between donor vesicles and the tBLM occurs in the outer leaflet at a rate nearly 2.5 times that of the inner leaflet, providing strong evidence for asymmetric tBLM assembly via vesicle exchange. Finally, we note that the phospholipid exchange with vesicles occurs noticeable slower than that for cholesterol. In 90 min, only ≈22% of outer leaflet composition is exchanged, suggesting that the $t_{1/2}$ value for the phospholipid transfer is at least 4−6 h.

dx.doi.org/10.1021/la304613a | *Langmuir* 2013, 29, 4320−4327

CONCLUSION

The fabrication of robust, low-defect density solid-supported phospholipid membranes is limited by the RSE method because water-miscible solvents are required, which precludes the incorporation of many important lipids. We show that the composition of tBLMs assembled by the RSE method can be modified by vesicle−tBLM material transfer, demonstrated here for lipids and cholesterol. The tBLM modification rate depends upon the component being transferred. For cholesterol, the transfer rates ($t_{1/2}$ < 60 min) were comparable to that observed for vesicle−vesicle ($t_{1/2} \approx$ 88 min), whereas transfer of DMPC to DOPC-completed tBLMs occurs much slower ($t_{1/2}$ = 4−6 h). Importantly, our data show the possibility of simultaneous transfer of several components.

ASSOCIATED CONTENT

Supporting Information

Estimation of the αHL channel density, estimation of the capacitance C_{mH} decrease because of a decrease of defectiveness, demonstration of simultaneous transfer of phospholipid and cholesterol from vesicles to tBLMs, NR data, and photo of the EIS six-vial measurement cell. This material is available free of charge via the Internet at http://pubs.acs.org.

AUTHOR INFORMATION

Corresponding Author

*Telephone: 370-5-2729186. Fax: 370-5-2729196. E-mail: gintaras.valincius@bchi.vu.lt.

Notes

Disclaimer: Certain commercial equipment, instruments, or materials are identified in this paper to specify the experimental procedure adequately. Such identification is not intended to imply recommendation or endorsement by the NIST, nor is it intended to imply that the materials or equipment are necessarily the best available for that purpose.

The authors declare no competing financial interest.

ACKNOWLEDGMENTS

The authors thank the British Science and Technology Facilities Council for granting access to the pulsed neutron source facilities through the usage of the European FP7 Transnational access program. Gintaras Valincius and Mindaugas Mickevicius thanks Dr. M. Skoda (ISIS, U.K.) for the extensive practical help and advice in carrying out the experiment RB1120347 at ISIS. This work has been supported by the Research Council of Lithuania (Contract MIP-096/2011) and was performed in part at the NIST Center for Nanoscale Science and Technology.

REFERENCES

(1) Knoll, W.; Naumann, R.; Friedrich, M.; Robertson, J. W. F.; Lösche, M.; Heinrich, F.; McGillivray, D. J.; Schuster, B.; Gufler, P. C.; Pum, D.; Sleytr, U. B. S. *Biointerphases* **2008**, *3*, FA125−FA135.
(2) Castellana, E. T.; Cremer, P. S. *Surf. Sci. Rep.* **2006**, *61*, 429−444.
(3) Sackmann, E.; Tanaka, M. *Trends Biotechnol.* **2000**, *18*, 58−64.
(4) Sackmann, E. *Science* **1996**, *271*, 43−48.
(5) Tamm, L. M.; McConnell, H. M. *Biophys. J.* **1985**, *47*, 105−113.
(6) Richter, R. P.; Berat, R.; Brisson, A. R. *Langmuir* **2006**, *22*, 3497−3505.
(7) Spinke, J.; Yang, J.; Wolf, H. *Biophys. J.* **1992**, *63*, 1667−1671.
(8) Plant, A. L. *Langmuir* **1993**, *9*, 2764−2767.
(9) McGillivray, D. J.; Valincius, G.; Vanderah, D. J.; Febo-Ayala, W.; Woodward, J. T *Biointerphases* **2007**, *2*, 21−33.
(10) Naumann, R.; Schiller, S. M.; Giess, F.; Grohe, B.; Hartman, K. B.; Karcher, I.; Köper, I.; Lubben, J.; Vasilev, K.; Knoll, W. *Langmuir* **2003**, *19*, 5435−5443.
(11) Achalkumar, A. S.; Bushby, R. J.; Evans, S. D. *Soft Matter* **2010**, *6*, 6036−6051.
(12) Raguse, B.; Braach-Maksvytis, B.; Cornell, A. B.; King, G. L.; Osman, P. D. J.; Pace, R. J.; Wieczorel, L. *Langmuir* **1998**, *14*, 648−659.
(13) Lang, H.; Duschl, C.; Vogel, H. *Langmuir* **1994**, *10*, 197−210.
(14) Vockenroth, I. K.; Ohm, K.; Robertson, J. W. F.; McGillivray, D. J.; Lösche, M.; Köper, I. *Biointerphases* **2008**, *3*, 68−73.
(15) Cornell, B. A.; Braach-Maksvytis, V. L. B.; King, L. B.; Osman, P. D. J.; Raguse, B.; Wieczorek, L.; Pace, R. J. *Nature* **1997**, *387*, 580−583.
(16) Bayley, H.; Cremer, P. S. *Nature* **2001**, *413*, 226−230.
(17) Budvytyte, R.; Valincius, G.; Niaura, G.; Voiciuk, V.; Mickevicius, M.; Stauffer, H.; Goh, H.-Z.; Shekhar, P.; Heinrich, F.; Shenoy, S.; Vanderah, D. J.; Lösche, M., manuscript in preparation.
(18) Chernomordik, L. V.; Kozlov, M. M. *Cell* **2005**, *123*, 375−382.
(19) Zhang, J.; Xue, R.; Ong, W.; Chen, P. *Biophys. J.* **2009**, *97*, 1371−1380.
(20) Tamm, L. K.; Crane, J.; Kiessling, V. *Curr. Opin. Struct.* **2003**, *13*, 456−466.
(21) Sudhof, T. C.; Rothman, J. E. *Science* **2009**, *323*, 474−477.
(22) Paleos, C. M.; Tsiourvas, D.; Sideratou, Z. *ChemBioChem* **2011**, *12*, 510−521.
(23) Cevc, G.; Richardsen, H. *Adv. Drug Delivery Rev.* **1999**, *38*, 207−232.
(24) Kunze, A.; Sjovall, P.; Kasemo, B.; Svedhem, S. J *J. Am. Chem. Soc.* **2009**, *131*, 2450−2451.
(25) Thomas, P. D.; Poznansky, M. J. *Biochem. J.* **1988**, *254*, 155−160.
(26) Lang, T.; Bruns, D.; Wenzel, D.; Riedel, D.; Holroyd, P.; Thiele, Ch.; Jahn, R. *EMBO J.* **2001**, *20*, 2202−2213.
(27) Heinrich, F.; Ng, T.; Vanderah, D. J.; Shekhar, P.; Mihailescu, M.; Nanda, H.; Lösche, M. *Langmuir* **2009**, *25*, 4219−4229.
(28) Wells, K.; Farooqui, A. A.; Liss, L.; Horrocks, L. A. *Neurochem. Res.* **1995**, *20*, 1329−1333.
(29) Shekhar, P.; Nanda, H.; Lösche, M.; Heinrich., F. *J. Appl. Phys.* **2011**, *110*, 102212−102216.
(30) Kirby, B. J.; Kienzle, P. A.; Maranville, B. B.; Berk, N. F.; Krycka, J.; Heinrich, F.; Majkrzak., C. F. *Curr. Opin. Colloid Interface Sci.* **2012**, *17*, 44−53.
(31) Boukamp, B. *Solid State Ionics* **1986**, *20*, 31−44.
(32) Valincius, G.; Meskauskas, T.; Ivanauskas, F. *Langmuir* **2012**, *28*, 977−990.
(33) McGillivray, D. J.; Valincius, G.; Heinrich, F.; Robertson, J. W. F.; Vanderah, D. J.; Febo-Ayala, W.; Ignatjev, I.; Lösche, M.; Kasianowicz, J. J. *Biophys. J.* **2009**, *96*, 1547−1553.
(34) Valincius, G.; Heinrich, F.; Budvytyte, R.; Vanderah, D. J.; McGillivray, D. J.; Sokolov, Y.; Hall, J. E.; Lösche, M. *Biophys. J.* **2008**, *95*, 4845−4861.
(35) Karatekin, E.; Sandre, O.; Guitouni, H.; Borghi, N.; Puech, P.-H.; Brochard-Wyart, F. *Biophys. J.* **2003**, *84*, 1734−1449.
(36) Ohki, S. *Biophys. J.* **1969**, *9*, 1195−1205.
(37) Bunce, A. S.; Hider, R. C. *Biochim. Biophys. Acta* **1974**, *363*, 423−427.
(38) Pan, J.; Tristran-Nagle, S.; Nagle, J. *Phys Rev. E: Stat., Nonlinear, Soft Matter Phys.* **2009**, *80* (021931), 1−12.
(39) Hung, W. C.; Lee, M. T.; Chen, F. Y.; Huang, H. W. *Biophys. J.* **2007**, *92*, 3960−3967.
(40) Starke-Peterkovic, T.; Turner, N.; Vitha, M. F.; Waller, M. P.; Hibbs, D. E.; Clarke, R. J. *Biophys. J.* **2006**, *90*, 4060−4070.
(41) Bruckner, R. J.; Mansy, S. S.; Ricardo, A.; Mahadevan, L.; Szostak, J. W. *Biophys. J.* **2009**, *97*, 3113−3122.
(42) Steck, T. L.; Ye, J.; Lange, Y. *Biophys. J.* **2002**, *83*, 2118−2125.
(43) Garg, S.; Ruhe, J.; Ludtke, K.; Jordan, R.; Naumann, C. A. *Biophys. J.* **2007**, *92*, 1263−1270.

(44) Ohvo-Rekilä, H.; Ramsted, B.; Leppimäki, P.; Slotte., J. P. *Prog. Lipid Res.* **2002**, *41*, 66−97.
(45) Demel, R. A.; Geurts van Kessel, W. S. M.; van Deenen., L. L. M. *Biochim. Biophys. Acta* **1972**, *266*, 26−40.
(46) Bezrukov, S. M.; Vodyanoy, I.; Brutyan, R. A.; Kasianowicz, J. J. *Macromolecules* **1996**, *29*, 8517−8522.
(47) Forti, S.; Menestrina, G. *Eur. J. Biochem.* **1989**, *181*, 767−773.